

An Improved Wall-climbing Robot Complete Coverage Path Planning Method for Wind Turbine Blade

Da Chen

School of Mechanical Engineering and Automation
Harbin Institute of Technology, Shenzhen
Shenzhen, China
neilchen98@163.com

Gang Yu

School of Mechanical Engineering and Automation
Harbin Institute of Technology, Shenzhen
Shenzhen, China
gangyu@hit.edu.cn

Shuchen Huang

School of Mechanical Engineering and Automation
Harbin Institute of Technology, Shenzhen
Shenzhen, China
zuzhsc@163.com

Abstract—In wind turbine blade maintenance, path planning for wall-climbing robots is a critical issue. The large size and complex curvature variations of turbine blades pose unique challenges to path planning. To address this problem, this study proposes an energy-consumption-based bio-inspired neural network method for complete coverage path planning. By considering the robot's energy consumption, this method better integrates height differences, angle differences, and distance differences between grid cells, optimizing the robot's energy expenditure on the map. The simulation results show that the algorithm can effectively handles the size and curvature variations of wind turbine blades, providing an efficient and reliable solution for the path planning of wall-climbing robots.

Keywords—Wind turbine blade, Complete coverage path planning, Energy consumption, Bio-inspired neural network

I. INTRODUCTION

With the rapid development of wall-climbing robot technology, these robots have been increasingly deployed in defect detection tasks for structures such as bridges, ship hulls, and wind turbine blades. Defect detection on wind turbine blades often necessitates operation in high-altitude and complex curved surface environments, where traditional manual inspection methods pose significant safety risks and are inefficient. Wall-climbing robots demonstrate high adaptability on wind turbine blades, enabling precise detection of surface defects without risking human injury and at a lower maintenance cost. For the extensive surface areas of wind turbine blades, automatic and efficient path planning is crucial for wall-climbing robots to autonomously execute defect detection tasks, thereby significantly improving inspection efficiency and reducing energy consumption.

Path planning algorithms for robots can be categorized into point-to-point path planning and area coverage path planning. The primary objective of point-to-point path planning is to find a collision-free path from the start point to the endpoint, whereas coverage path planning aims to determine a path that traverses all points within an area or volume while avoiding obstacles. For wall-climbing robots tasked with defect detection on wind

turbine blades, the path planning algorithm falls under coverage path planning. Coverage path planning algorithms can be divided into cell decomposition methods, grid-based methods, multi-robot methods, etc.[1][2][3]. However, most of these focus on two-dimensional plane coverage issues and seldom consider the impact of three-dimensional terrain on path planning, often neglecting height differences in the map environment, which increases the robot's energy consumption. Conversely, three-dimensional maps present challenges of high computational complexity and intricate planning. In this context, a 2.5D map, which combines a two-dimensional map with height information, can consider the impact of height on energy consumption while maintaining low computational requirements.

A unique aspect of the wind turbine blade inspection task is that defects detected by the wall-climbing robot on the blade surface act as real-time obstacles, similar to a mine-sweeping problem (i.e., finding mines in a locally unknown map). The planning path of the wall-climbing robot must efficiently cover the entire work area while avoiding defects on the blade. Bio-inspired neural networks, inspired by biological behaviors, can handle environmental changes or uncertainties such as suddenly appearing obstacles by processing sensor data and environmental information in real-time and making quick planning decisions. Additionally, bio-inspired neural networks ensure low computational burden, making them suitable for use in embedded devices. Enhancements to their heuristic functions can improve performance and achieve more optimal solutions.

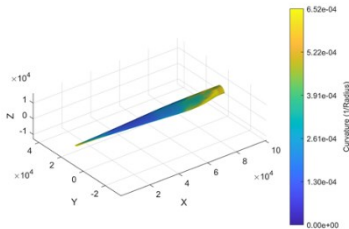
To address the environmental changes that may occur on wind turbine blades and consider the height variations on the blade surface, we propose an energy consumption model for wall-climbing robots that incorporates angle differences, height differences, and distance differences. Based on this model, we improve the bio-inspired neural network to overcome the limitations of traditional two-dimensional plane coverage path planning algorithms, thereby reducing the energy consumption of wall-climbing robots on wind turbine blades.

The rest of this paper is organized as follows. Section II provides a detailed analysis of key research areas on wind turbine blades, extraction of height information, and construction of a 2.5D grid map[4], which serves as the basis for establishing the energy consumption model for the wall-climbing robot. A bio-inspired neural network-based coverage path planning algorithm that considers the energy consumption model is then developed. Section III presents a set of simulations to validate the advantages of the proposed algorithm compared to traditional two-dimensional plane coverage path planning algorithms. Finally, Section IV concludes the paper.

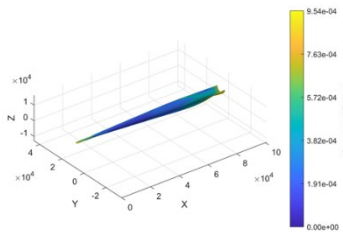
II. THE IMPROVED BINN COMPLETE COVERAGE PATH PLANNING BASE ON ROBOT ENERGY CONSUMPTION MODEL

A. Wind Turbine Blade typical Region Analysis

To simulate the actual working environment on wind turbine blades and in consideration of the computational results and structural design requirements, areas with significant curvature and where wall-climbing robot adhesion is more challenging were selected as key research focuses. The large size and complex surface curvature variations of wind turbine blades necessitate this focus. The curvature variations on the surface of the wind turbine blade are illustrated in Fig. 1. Brightly colored regions, indicating areas with dramatic curvature changes, often represent bottlenecks in path planning. As shown in the figure, the blade surface generally has small curvature, with larger curvature areas primarily concentrated at the blade root and tip. The lower half of the blade has a slightly larger curvature compared to the upper half and thus should be considered a priority area in the study.



(a) The curvature of the upper half of the blade



(b) The curvature of the lower half of the blade

Fig. 1. Curvature variation on the surface of wind turbine blades

For the two typical types of damage on wind turbine blades, their occurrence areas are shown in Fig. 2. Typically, the damage at the blade tip region is erosion, where the curvature is larger. The typical defect between the root region and two-thirds of the blade length is cracking, where the curvature is smaller.

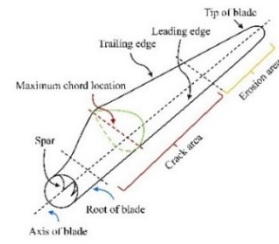
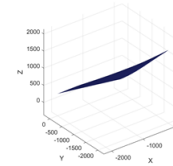
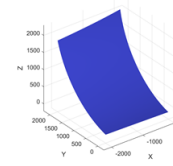


Fig. 2. Vulnerable areas of the blade

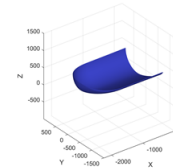
Based on the occurrence areas and curvature conditions of these two different types of damage, the typical operational regions of the wind turbine blade are extracted. The extracted typical erosion and crack regions are shown in Fig. 3.



(a) Typical region at the root of the blade



(b) Typical region in the middle of the blade



(c) Typical region at the tip of the blade

Fig. 3. Extracted three typical regions of the blade

B. Extraction of Height Information in typical Regions

In full coverage path planning tasks, traditional 2D grid maps typically contain only planar positional information and cannot fully reflect the complexity of real-world environments. In practical applications, environments are often three-dimensional, with various height variations such as slopes, steps, and obstacles. These height variations significantly impact path planning, and ignoring height information can result in planned paths that are infeasible in actual execution, potentially leading to safety hazards. Generally, full coverage path planning for robots only considers the impact of positional changes in two-dimensional coordinates. In this paper, considering the specificity of the working environment, the surface of wind turbine blades is not a flat plane but has certain height and curvature variations. When a legged wall-climbing robot crawls on the surface of a wind turbine blade, its movement needs to be combined with its adhesion state. By incorporating height

information, paths can be planned more accurately to reduce redundant coverage and missed areas, thereby improving task efficiency and resource utilization.

We first project the typical regions of the blade onto the xy -plane and divide the xy -plane into grids. For each grid, we obtain the z -coordinate of the center point on the corresponding surface by using the four corner points of the grid. These center points are then extracted as point cloud information.

C. Construction of A 2.5D Grid Map

A 2.5D grid map is a representation method that combines two-dimensional planar positions with height information. Each grid cell contains not only planar coordinates but also height values. By incorporating height information, path planning algorithms can better avoid obstacles, select optimal paths, and prevent unnecessary climbing or descending, thus improving planning efficiency and reducing energy consumption. For the typical regions mentioned in the previous section, it is necessary to first rasterize the environment map and assign different values to the states of each grid cell to construct a two-dimensional grid map.

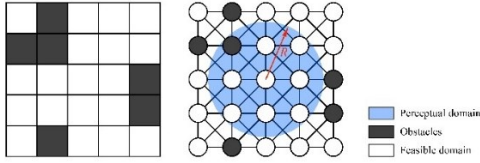


Fig. 4. Correspondence between the 2D grid map and the Biological Inspired Neural Network (BINN)

The correspondence between the 2D grid map and the Biological Inspired Neural Network (BINN) is shown in Fig. 4. A corresponding 2D neural network is constructed from the 2D grid map, where each grid in the grid map is represented by a neuron in the neural network. Each neuron can sense other neurons within a radius R to determine the next move direction. Based on this 2D grid map, height information for each grid is acquired. The height represented by each grid is stored in the grid map, constructing 2.5D grid maps for the typical mid-section region, as shown in Fig. 5.

1738	1775	1785	1784	1778	1782	1811	1810	1820	1818	1828	1880	1883	1871	1881	1884	1900	1900	1914	1918	1912
1829	1850	1859	1855	1841	1852	1816	1876	1872	1861	1869	1902	1902	1908	1913	1921	1928	1932	1927	1922	1912
1834	1842	1845	1847	1843	1846	1386	1386	1386	1386	1386	1382	1385	1387	1370	1374	1378	1382	1384	1385	1384
1168	1168	1171	1172	1173	1174	1176	1177	1178	1180	1181	1183	1185	1187	1188	1191	1193	1195	1196	1198	1200
1031	1031	1032	1032	1033	1033	1034	1035	1035	1036	1037	1038	1040	1041	1042	1044	1044	1045	1047	1049	1049
800	800	800	800	800	800	800	800	800	800	800	800	800	800	800	800	800	800	800	800	800
801	800	800	798	798	798	798	798	798	798	797	798	798	798	798	798	798	798	798	798	800
702	702	701	701	700	699	698	698	697	697	696	696	696	695	695	695	695	695	695	695	695
616	615	612	611	610	610	609	608	607	606	606	605	604	604	603	603	602	602	601	601	601
534	533	532	531	530	529	527	526	525	524	523	522	522	521	520	519	518	518	517	516	516
462	460	459	458	457	455	454	453	451	450	449	448	447	446	445	444	443	442	441	440	440
386	384	383	381	380	380	381	380	384	383	382	380	379	378	377	374	373	372	371	371	371
306	304	303	301	300	300	306	305	303	302	300	319	317	316	315	313	312	310	309	308	308
281	280	278	276	275	273	271	270	268	267	265	263	262	260	259	257	255	254	253	251	251
200	201	209	207	205	204	202	200	200	200	217	216	215	212	210	208	207	205	203	202	200
188	187	185	183	181	180	178	176	174	172	171	169	167	165	163	161	160	158	156	154	154
148	147	145	144	142	140	138	136	134	133	131	129	127	125	123	121	119	117	115	113	113
114	113	110	108	107	106	104	102	100	98	96	94	92	90	88	86	84	82	80	77	77
83	81	80	78	76	75	74	73	71	68	65	63	61	59	57	55	54	52	49	46	46
57	55	53	52	50	48	47	46	44	41	38	36	34	32	30	28	26	24	22	19	19

Fig. 5. 2.5D grid map of the typical mid-section region

D. Establishment of the Energy Consumption Model

When operating on wind turbine blades, due to the immense size of the blades and the limited mobility of wall-climbing robots, it is necessary to manage the robot's endurance time on

the blades. The energy consumption of the wall-climbing robot directly affects its operational efficiency and continuous working time. By establishing an energy consumption model, the required energy for the robot to complete full coverage defect detection on the wind turbine blade can be accurately predicted. This ensures that the robot operates within a safe energy consumption range, preventing safety incidents such as adhesion failure or falling due to excessive energy consumption. This, in turn, optimizes power management strategies, extends the robot's working time, and reduces the need for frequent recharging or battery replacement. Additionally, the energy consumption model provides important references for path planning. By analyzing the energy consumption of different paths, the path with the lowest energy consumption can be chosen, ensuring that the robot can efficiently complete blade inspection and maintenance tasks.

To perform reasonable full coverage path planning for the wall-climbing robot, it is necessary to establish its energy consumption model. The wall-climbing robot designed in this paper uses a four-legged pneumatic pump adsorption system to adhere to the surface of the wind turbine blade. The kinematic diagram of a single leg mechanism of the robot is shown in Fig. 6. The energy consumption of the wall-climbing robot during inspection on the wind turbine blade surface mainly comes from the robot's control system and motion system.

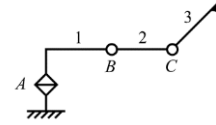


Fig. 6. Kinematic diagram of the robot's single-leg mechanism

As shown in Fig. 7, the wall-climbing robot can move in eight directions, and its main movement modes can be divided into: 1) rotation mode and 2) linear movement mode.

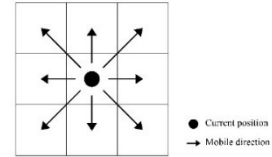


Fig. 7. Kinematic diagram of the robot's single-leg mechanism

The robot's movement in the eight directions can be decomposed into a combination of these two movement modes. Let t_r be the time taken for the wall-climbing robot to rotate, t_s be the time taken for the wall-climbing robot to move linearly in a straight direction, P_c be the power of the wall-climbing robot's control module, E_c be the energy consumed by the control module, E_m be the energy consumed by the motion module, and E_{sum} be the total energy consumption of the wall-climbing robot.

$$E_{sum} = E_c + E_m = P_c(t_r + t_s) + E_m \quad (1)$$

Since the wall-climbing robot's movement in eight directions can be decomposed into a combination of rotation mode and linear movement mode, let the energy consumption in rotation

mode be E_r and the energy consumption in linear movement mode be E_s , namely:

$$E_m = E_r + E_s \quad (2)$$

The magnitudes of E_r and E_s are primarily related to the rotation angle α , the linear movement distance d , and the height difference Δh between two grids, namely:

$$E_m = E_r(\alpha, d, \Delta h) + E_s(\alpha, d, \Delta h) \quad (3)$$

Let the rotation angles of joints A, B, and C be $\theta_1, \theta_2, \theta_3$ respectively. To ensure that the end effector always remains vertical, it is stipulated that the rotation angle of joint C is equal in magnitude but opposite in direction to that of joint B, i.e. $\theta_3 = -\theta_2$. The lengths of links 1, 2 and 3 are l_1, l_2, l_3 respectively. The geometric relationship of a single leg is shown in Fig. 8.

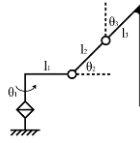


Fig. 8. Geometric relationship of the robot's single leg

The relationship between the rotation angles and the lengths of the links can be derived as follows:

$$\begin{cases} \alpha = \theta_1 \\ d = l_1 \sin \theta_1 \\ \Delta h = l_2 \sin \theta_2 \end{cases} \quad (4)$$

When the wall-climbing robot is in rotation mode, the rotation angle α is the rotation angle θ_1 of joint A, and the linear movement distance $d = 0$. Set θ_{r2} and θ_{r3} to fixed values. When θ_{r1} is not zero, i.e., the wall-climbing robot is in rotation mode, make it effective; otherwise, set them all to zero. By controlling with a very small positive number ϵ , the rotation angles of each joint can be obtained as follows:

$$\begin{cases} \theta_{r1} = \alpha \\ \theta_{r2} = (\pi/6) \times (|\theta_{r1}|/|\theta_{r1}| + \epsilon) \\ \theta_{r3} = -(\pi/6) \times (|\theta_{r1}|/|\theta_{r1}| + \epsilon) \end{cases} \quad (5)$$

When the wall-climbing robot is in linear movement mode, the rotation angle α is determined by the required linear movement distance d , and the rotation angle θ_{s2} of joint B is determined by the height difference between two grids. The rotation angles of each joint can be obtained as follows:

$$\begin{cases} \theta_{s1} = \sin^{-1} \theta(d/l_1) \\ \theta_{s2} = \sin^{-1} \theta(\Delta h/l_2) \\ \theta_{s3} = -\sin^{-1} \theta(\Delta h/l_2) \end{cases} \quad (6)$$

Therefore, τ represents the joint motor torque and η represents the joint motor efficiency, the energy consumed by the wall-climbing robot's motion module can be obtained as:

$$E_m = E_r + E_s = \sum_{i=1}^3 \left(\frac{\tau \times \theta_{ri}}{\eta} \right) + \sum_{i=1}^3 \left(\frac{\tau \times \theta_{si}}{\eta} \right) \quad (7)$$

The movement relationship between the robot as a whole and its individual legs is considered. The total energy consumed by the wall-climbing robot to move in any of the eight directions is:

$$E_{sum} = 8P_c + 4(\tau/\eta) \sum_{i=1}^3 (\theta_{ri} + \theta_{si}) \quad (8)$$

III. SIMULATION AND DISCUSSION

Biologically Inspired Neural Network (BINN) performs full coverage path planning by mimicking the behavior of biological systems. Through the neural network model, it enables the robot to autonomously navigate and cover tasks in complex environments. BINN utilizes the activities and interactions of neurons to simulate the navigation mechanisms of biological organisms, possessing adaptive and dynamic planning capabilities. The BINN basic shunting equation is as follows[5]:

$$\frac{dX_i}{dt} = -AX_i + (B - X_i)[[I_i]^+ + \sum_{j=1}^n \omega_{ij}[X_j]^+] - (D + X_i)[I_i]^- \quad (9)$$

Where A is the decay rate of neuronal activity, B and D are the upper and lower limits of neuronal activity, and n is the number of neighboring neurons within the sensing radius RR of the $i - th$ neuron. In this paper, $R = 2$, meaning the states of the eight neighboring neurons within the neighborhood are used as reference values[6]. I_i represents the external input, which is expressed as follows:

$$f(x) = \begin{cases} E, & \text{Uncovered area} \\ -E, & \text{Obstacle area} \\ 0, & \text{Covered area} \end{cases} \quad (10)$$

The overall process of full coverage path planning based on BINN takes map information and the robot's positioning information as inputs and outputs a complete path. First, the input information is initialized, a grid map is created, and a corresponding neural network is constructed to represent the state of the grid cells. The robot starts from the initial position to cover the area, determining the next target cell through a priority heuristic formula. After the robot moves to the next target cell, the target cell becomes the current cell, and the current cell is marked as covered, updating the grid map[7]. When the robot finds that all eight surrounding grids have been traversed, it indicates that the robot is trapped. Based on the current traversal situation of the entire grid network, it chooses to either escape the dead zone to an undetected grid or end the robot's inspection activity[8].

A. Mission Scenarios

By proportionally scaling the typical middle region of a blade, a 2.5D grid map is constructed as the simulated environment for the robot. The grid map is sized 20×20 . The robot starts from the same position, and the movement ends when all grids have been traversed. The original BINN algorithm is compared with the energy consumption model-improved BINN algorithm.

B. Simulation Result and Discussion

By simulating the traversal of the robot on the grid map using the current BINN algorithm and the energy-consumption-

considering BINN algorithm, both algorithms are able to successfully complete the full coverage path planning.

The changes in neuronal activity during the grid traversal are shown in Fig. 9, compared to the neuronal activity after the grid traversal is completed, as shown in Fig. 10.

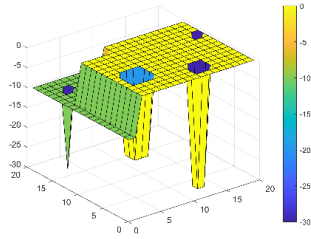


Fig. 9. The neuronal activity during the grid traversal

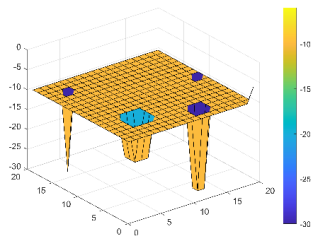


Fig. 10. The neuronal activity after the grid traversal is completed

Through simulation, the full coverage path of the traditional BINN algorithm can be obtained as shown in Fig. 11, and the full coverage path of the energy-consumption-considering BINN algorithm is shown in Fig. 12.

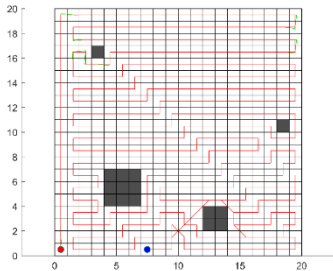


Fig. 11. Full coverage path of the traditional BINN algorithm

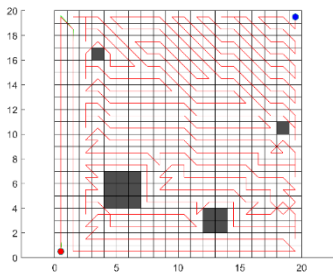


Fig. 12. Full coverage path of the energy-consumption-considering BINN algorithm

By comparison, we can obtain the evaluation data for the traditional BINN algorithm and the energy-consumption-considering BINN algorithm. We mainly consider total path length, repeat rate, and energy consumption. The data obtained is shown in Table 1.

By comparison, we can see that although the total path length and repeat rate of the BINN algorithm increase when energy consumption is considered, the energy consumed is actually less due to the consideration of height and energy consumption information. This indicates that when the BINN algorithm takes energy consumption into account, it can achieve better results in terms of the robot's endurance and work efficiency.

TABLE I. PERFORMANCE EVALUATION

BINN Algorithm	Evaluation Metrics		
	Energy consumption	Path length	Repeat rate
Traditional	2259.94	397.48	0.03
Improved	1775.19	439.56	0.14

IV. CONCLUSION

Our research demonstrates the substantial benefits of integrating energy consumption considerations into BINN-based path planning algorithms. The improved algorithm not only ensures complete coverage but also optimizes energy usage, thereby extending the operational lifespan and efficiency of robotic systems. These findings provide valuable insights for future developments in robotic path planning, emphasizing the importance of energy-aware strategies in enhancing performance and sustainability.

REFERENCES

- [1] ACAR E U, P. B. Jackson, and J. C. Smith, "Morse Decompositions for Coverage Tasks," *International Journal of Robotics Research*, vol. 21, no. 4, pp. 331-344, 2002.
- [2] LUO C, YANG S X, "A Solution to Vicinity Problem of Obstacles in Complete Coverage Path Planning," in *Proceedings of the International Conference on Robotics and Automation, IEEE, 2002*, pp. 612-617.
- [3] MAZA and A. OLLERO, "Multiple UAV cooperative searching operation using polygon area decomposition and efficient coverage algorithms," in *Distributed Autonomous Robotic Systems 6*, Tokyo: Springer Japan, 2007, pp. 221-230.
- [4] P. Fankhauser and M. Hutter, "A Universal Grid Map Library: Implementation and Use Case for Rough Terrain Navigation," in *Robot Operating System (ROS): The Complete Reference (Volume 1)*, A. Koubaa, Ed. Springer, 2016, ch. 5.
- [5] S. X. Yang and C. Luo, "A neural network approach to complete coverage path planning," *IEEE Transactions on Systems, Man, and Cybernetics, Part B (Cybernetics)*, vol. 34, no. 1, pp. 718-724, 2004.
- [6] M. A. V. J. Muthugala, S. M. B. P. Samarakoon, and M. R. Elara, "Toward energy-efficient online complete coverage path planning of a ship hull maintenance robot based on Glasius bio-inspired neural network," *Expert Systems with Applications*, vol. 187, 2022, Art. no. 115940.
- [7] P. Manoonpong, L. Patanè, et al., "Insect-inspired robots: bridging biological and artificial systems," *Sensors*, vol. 21, no. 22, 2021, Art. no. 7609.
- [8] B. Sun, D. Zhu, C. Tian, et al., "Complete coverage autonomous underwater vehicles path planning based on Glasius bio-inspired neural network algorithm for discrete and centralized programming," *IEEE Transactions on Cognitive and Developmental Systems*, vol. 11, no. 1, pp. 73-84, 2018.